

Effects of Gd, Co, and Ni doping in $\text{La}_{2/3}\text{Ca}_{1/3}\text{MnO}_3$: Resistivity, thermopower, and paramagnetic resonance

Mark Rubinstein, D. J. Gillespie, and John E. Snyder
U.S. Naval Research Laboratory, Washington, D.C. 20390

Terry M. Tritt

Clemson University, Clemson, South Carolina 29634

(Received 19 February 1997; revised manuscript received 30 April 1997)

The effect of elemental substitutions on the properties of the ferromagnetic, conducting, highly magnetoresistive compound $\text{La}_{2/3}\text{Ca}_{1/3}\text{MnO}_3$ has been studied. The results of Co doping and Ni doping on the Mn site and Gd doping on the La site are reported. These compounds were investigated by x-ray diffraction, magnetization measurements, resistivity measurements, thermopower measurements, and by paramagnetic resonance. The result of replacing La by Gd atoms is to lower the ferromagnetic (or metal-insulator) transition temperature, an effect which is shown to be due to bond bending caused by the lattice adjusting to the size differential between the La and Gd ions. On the other hand, the reduction of the magnetic transition temperature when Mn ions are replaced with Co or Ni ions is *not* attributed to changes in the size of the ions. Instead, we ascribe the lowering of the ferromagnetic transition temperature to a weakening of the double-exchange interaction between two unlike ions. The resistivity and Seebeck coefficient in these materials have been investigated as a function of elemental substitution. The magnetic polaron theory of Zhang is used, phenomenologically, to provide a quantitative explanation of these transport properties. In addition, the effect of these elemental substitutions on the linewidths of the paramagnetic resonances is studied and is discussed in terms of exchange narrowing and spin-lattice relaxation. [S0163-1829(97)02634-9]

I. MOTIVATION

Compounds which are high-temperature superconductors (HTS's) and display colossal magnetoresistivity (CMR) have much in common. Both materials are transition-metal oxides containing rare-earth metals and incorporating alkaline metals acting as hole dopants. Both are brittle ceramics, processed in similar ways and subject to similar materials problems. (The major difference between these two types of materials, besides the obvious fact that one is a superconductor and the other a magnet, lies in the transition metal employed—copper versus manganese—and in the structure—two-dimensional layered versus cubic perovskite.)

Because of their similarities, we have reasoned that those experiments which had, in the past, proved useful for the HTS's might also be instructive for CMR. In particular, we were attracted to the study of elemental substitutions, which had, even in the earliest days, proved to be valuable in the study of the HTS's.

For example, the effect of the rare-earth replacement of La in LaSrCuO or of Y in YBaCuO has a surprisingly small effect on the superconducting transition temperature (with Pr proving to be an interesting exception¹). Contrariwise, paramagnetic substitutions for copper in HTS compounds showed a profound lowering of the transition temperature due to the pair-breaking interaction with the transition-metal replacements.² Replacement of Cu with nonmagnetic Zn (a nonmagnetic substitution) depressed the superconducting transition temperature more than any other Cu elemental substitution—yet another unexpected result. The effect of substituting Pr for Y or of Zn for Cu, although deleterious to

superconductivity, is expected to provide important clues concerning the elusive mechanism of high-temperature superconductivity. For this reason, we have opted to study the effect of substitutions in the *manganites* in order to obtain clues concerning the mechanism of *colossal magnetoresistance*.

II. INTRODUCTION

In this paper, we will discuss our investigation concerning the effect of elemental substitutions on the CMR material $\text{La}_{2/3}\text{Ca}_{1/3}\text{MnO}_3$. We have substituted Gd for La, Co for Mn, and Ni for Mn in the compound $\text{La}_{2/3}\text{Ca}_{1/3}\text{MnO}_3$, by manufacturing a series of samples with the formulas $(\text{La}_{1-x}\text{Gd}_x)_{2/3}\text{Ca}_{1/3}\text{MnO}_3$, $\text{La}_{2/3}\text{Ca}_{1/3}(\text{Mn}_{1-x}\text{Co}_x)\text{O}_3$, and $\text{La}_{2/3}\text{Ca}_{1/3}(\text{Mn}_{1-x}\text{Ni}_x)\text{O}_3$, with $x=0.0, 0.25, 0.50, 0.75$, and 1.0 . (Although we refer to these perovskites as “ O_3 ,” no effort beyond examining their magnetic transition temperature and examining the x-ray-diffraction patterns was made to verify the oxygen stoichiometry.) These samples, made by the conventional ceramics “shake and bake” route,³ were heated to 1300°C under oxygen several times, after several intermediate grindings and pressings. The powder pattern x rays of the resulting powders with Co and Ni substitutions are shown in Fig. 1. (Most of the structure in the individual lines is caused by orthorhombic or tetragonal distortions⁴ in the material where the actual unit cell is composed of several primitive $\text{La}_{2/3}\text{Ca}_{1/3}\text{MnO}_3$ cells. These distortions will be discussed at length in a subsequent section.) Subsequently, these bulk samples were used as targets to produce thin films by utilizing pulsed laser deposition. Both bulk samples and thin films were investigated.

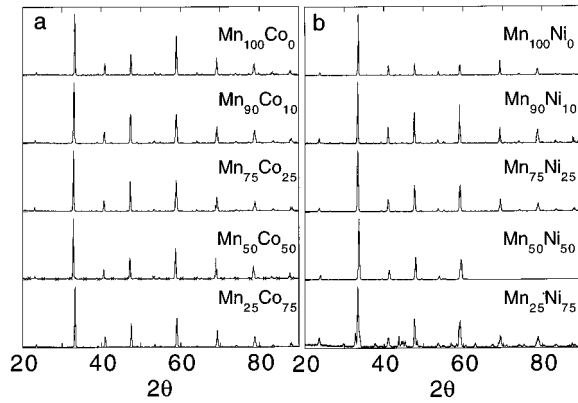


FIG. 1. Powder x-ray-diffraction spectra of polycrystalline, ceramic (a) $\text{La}_{2/3}\text{Ca}_{1/3}(\text{Mn}_{1-x}\text{Co}_x)\text{O}_3$ and (b) $\text{La}_{2/3}\text{Ca}_{1/3}(\text{Mn}_{1-x}\text{Ni}_x)\text{O}_3$.

Before discussing our results on these samples of $(\text{La}_{1-x}\text{Gd}_x)_{2/3}\text{Ca}_{1/3}\text{MnO}_3$, $\text{La}_{2/3}\text{Ca}_{1/3}(\text{Mn}_{1-x}\text{Co}_x)\text{O}_3$, and $\text{La}_{2/3}\text{Ca}_{1/3}(\text{Mn}_{1-x}\text{Ni}_x)\text{O}_3$, it is well to indicate, now, what is already known concerning the *end points* of each of these substitutional series. (1) The low-temperature phase of $\text{La}_{2/3}\text{Ca}_{1/3}\text{MnO}_3$ is (of course) a double-exchange ferromagnetic metal,⁵ whereas we shall subsequently show in this paper that $\text{Gd}_{2/3}\text{Ca}_{1/3}\text{MnO}_3$ is an insulating spinglass at low temperatures. (2) The low-temperature phase of $\text{La}_{2/3}\text{Ca}_{1/3}\text{CoO}_3$ has recently been also shown to be a double-exchange ferromagnetic metal.⁶ (3) The low-temperature phase of LaNiO_3 is a Pauli-paramagnetic metal⁷ from which we can extrapolate that $\text{La}_{2/3}\text{Ca}_{1/3}\text{NiO}_3$ is also a Pauli paramagnet, since it contains more carriers. We were, however, unsuccessful in manufacturing single-phase specimens of several of these end-point materials in this study.

In the present paper, several techniques have been used to determine the effect of these elemental substitutions on the fundamental properties of these CMR materials. Magnetic measurements and electrical-conductivity measurements were utilized to determine the phase diagrams. Thermopower and conductivity measurements were used to test theories of magnetic polaron conduction. Finally, electron paramagnetic resonance was employed to examine the nature of the exchange interactions and relaxation mechanisms at temperatures above the Curie point.

We have chosen to discuss the effects of Gd substitutions on the rare-earth site and the effects of Co/Ni substitutions on the transition-metal site in one medium-length paper, rather than in two small papers. By so doing, we can present a more coherent explanation of the electron paramagnetic resonance (EPR) linewidth and its dependence on elemental substitutions, and we may contrast the different effects of Co, Ni, and Gd substitution on the linewidth. It is also useful to contrast the different mechanisms which are responsible for the depression of the Curie temperatures in the three cases. The rare-earth substitutions are discussed in Secs. III–V, while the transition-metal substitutions are discussed in Secs. VI–X.

For reasons of completeness, we have also included some transport data and an interpretation previously reported by Jaime *et al.*⁸ on the Gd-doped samples discussed herein.

III. $(\text{La}_{1-x}\text{Gd}_x)_{2/3}\text{Ca}_{1/3}\text{MnO}_3$: REPLACEMENT OF La BY Gd

The initial reports on colossal magnetoresistance were perplexing to those of us who were unfamiliar with the literature on “tolerance factors.” It has been found that the magnetic and electrical properties of the doped rare-earth manganites—as typified by the metal-insulator or ferromagnetic-paramagnetic transition temperature—strongly depended on which trivalent rare-earth or the divalent alkali metal was used. This seemed surprising because of the weak sensitivity of the HTS’s superconducting transition to most rare-earth types. Utilizing a concept of the tolerance factor—first developed by Goldschmidt in the 1930’s—Hwang *et al.*⁹ demonstrated that the rare earth exerts an effect on the metal-insulator transition temperature primarily by virtue of its ionic radius.

In the undoped perovskite lattice LaMnO_3 , the Mn ions occupy the *B* sites and are surrounded by oxygen octahedra, which share corners to form a three-dimensional network, while the La ions occupy the *A* sites between these octahedra. The tolerance factor *t* is defined by

$$t = \frac{(d_{A-O})}{\sqrt{2}(d_{B-O})}, \quad (1)$$

where d_{B-O} is the Mn-O distance and d_{A-O} is the rare-earth site-oxygen site distance. *t* is a characterization of the size mismatch that occurs when the *A*-site ions are too small to fill the space in the three-dimensional network of MnO_6 octahedra. For a perfect size match ($t=1$), the Mn-O-Mn bond angle θ is 180° . For $t < 1$, the octahedra tilt and rotate to reduce the excess space around the *A* site, resulting in $\theta < 180^\circ$. Since the electronic overlap strongly depends on θ , the ferromagnetic transition temperature will decrease whenever the average rare-earth ionic radius decreases—for example by substituting a heavy rare-earth ion for a light La ion.

Hwang *et al.* proceeded to construct a phase diagram of temperature vs tolerance factor by investigating compounds of the form $A_{0.7}B_{0.3}\text{MnO}_3$, where *A* is a combination of trivalent rare earth ions and *B* is a divalent alkali-earth ion. In this series, the tolerance factor is systematically varied, while the hole carrier doping is fixed at its optimum value, $\sim 30\%$. Hwang *et al.* (primarily) investigated the series of samples represented by the formulas $\text{La}_{0.7-x}\text{Pr}_x\text{Ca}_{0.3}\text{MnO}_3$ and $\text{La}_{0.7-x}\text{Y}_x\text{Ca}_{0.3}\text{MnO}_3$. Their phase diagram is reproduced in Fig. 2, onto which we have superposed our results for $(\text{La}_{1-x}\text{Gd}_x)_{2/3}\text{Ca}_{1/3}\text{MnO}_3$ (represented by the large solid circles). Our results—described below—on the Gd-substituted compounds agree well with the general phase diagram proposed by Hwang *et al.* [excepting the fact that we find a spin-glass phase (SGI) where Hwang *et al.* find a ferromagnetic insulator phase] and supports the assertion that the transition temperature in Gd-substituted manganites is primarily determined by changes in the average size of the rare-earth ion.

We have manufactured a series of compounds with the formula $(\text{La}_{1-x}\text{Gd}_x)_{2/3}\text{Ca}_{1/3}\text{MnO}_3$ ($x=0, 0.25, 0.50, 0.75$, and 1.0) in order to confirm the phase diagram of Fig. 2. Figure 3 displays the behavior of the magnetization as a

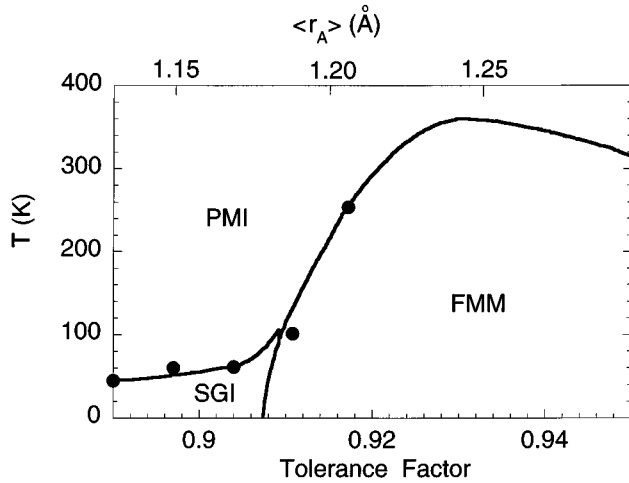


FIG. 2. Phase diagram of temperature vs tolerance factor for the system $A_{0.7}B_{0.3}\text{MnO}_3$, where A is a trivalent rare-earth ion and B is a divalent alkali-earth ion [after Hwang *et al.* (Ref. 9)]. Superimposed black circles represent the data on $(\text{La}_{1-x}\text{Gd}_x)_{2/3}\text{Ca}_{1/3}\text{MnO}_3$ from the present paper. The portion on the diagram labeled SGI represents a spin-glass-like phase for $(\text{La}_{1-x}\text{Gd}_x)_{2/3}\text{Ca}_{1/3}\text{MnO}_3$.

function of temperature for bulk samples. The $x=0$ and $x=0.25$ samples have ferromagnetic transitions close to the “metal-insulator transition” at the maximum of the resistivity versus temperature curve, observed in measurements of the resistivity versus temperature in these samples. The remaining samples are spin glasses (as determined by the presence of an irreversibility peak at low temperatures) and display only insulator-type behavior. Very similar effects are observed in the thin films. There are the data which are plotted on the phase diagram of Fig. 2. In Fig. 2 the tolerance factor (or equivalently the average A -site ionic radius, associated with each composition) is calculated from tabulated values, using the same coordination numbers as Ref. 8. Gd is seen to have a profound effect on both the metallic and magnetic properties of the Mn perovskite. Between 25% and 50% Gd substitution for La results in an insulating spin glass. As we have discussed, this effect is primarily due to the size difference between the La and Gd ions—the “lan-

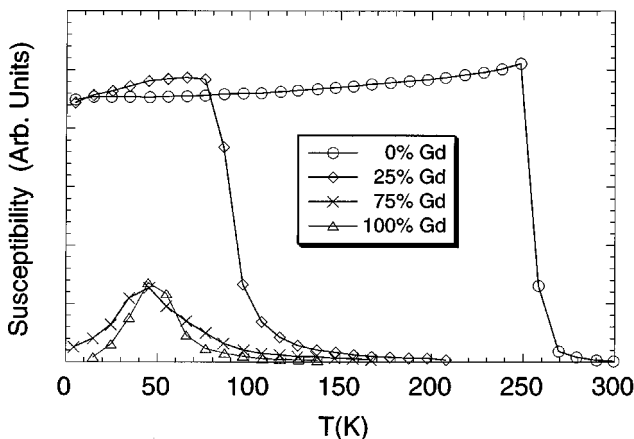


FIG. 3. Temperature dependence of magnetization obtained at an applied magnetic field of 30 G for bulk $(\text{Gd}_x\text{La}_{1-x})_{2/3}\text{Ca}_{1/3}\text{MnO}_3$, $x=0.0, 0.25, 0.50, 0.75$, and 1.0.

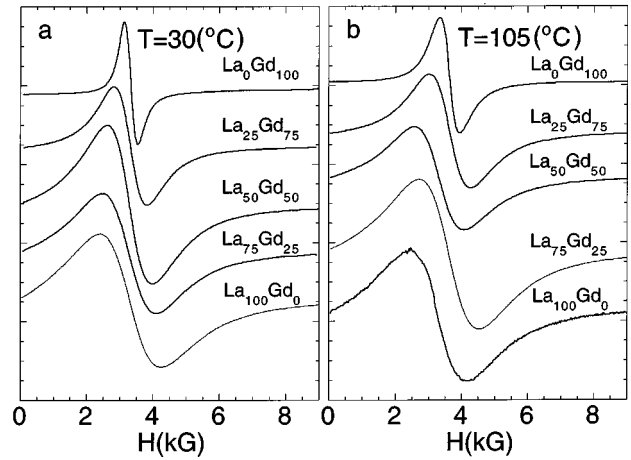


FIG. 4. Room-temperature and 105 °C electron-paramagnetic-resonance (EPR) absorption derivative spectra of bulk $(\text{La}_{1-x}\text{Gd}_x)_{2/3}\text{Ca}_{1/3}\text{MnO}_3$, $x=0.0, 0.25, 0.50, 0.75$, and 1.0.

thanide contraction”—and the manner with which the lattice adjusts to this size differential.

IV. PARAMAGNETIC RESONANCE (La-Gd)

In addition to magnetism and resistivity measurements, we have performed electron paramagnetic resonance studies on these compounds. We initially chose to substitute Gd for La because Gd has no orbital angular momentum and ought not to contribute excessively to the spin relaxation. (Later, however, we concluded that the contribution of Gd to the paramagnetic resonance linewidth was similar to that of other rare-earth elements.) In Fig. 4 we display the electron-paramagnetic-resonance absorption-derivative spectra for the five samples of polycrystalline $(\text{La}_{1-x}\text{Gd}_x)_{2/3}\text{Ca}_{1/3}\text{MnO}_3$ taken at room temperature (23 °C and 105 °C). Both temperatures are within the paramagnetic phase of the samples. The spectral linewidth is plotted in Fig. 5(b) as a function of Gd concentration; the linewidth of $\text{La}_{2/3}\text{Ca}_{1/3}\text{MnO}_3$ is plotted as a function of temperature in Fig. 5(a). The following results apply to the resonance of these manganite samples in the paramagnetic phase: (1) The linewidth, moderately small in the pure La sample, increases rapidly with Gd concentra-

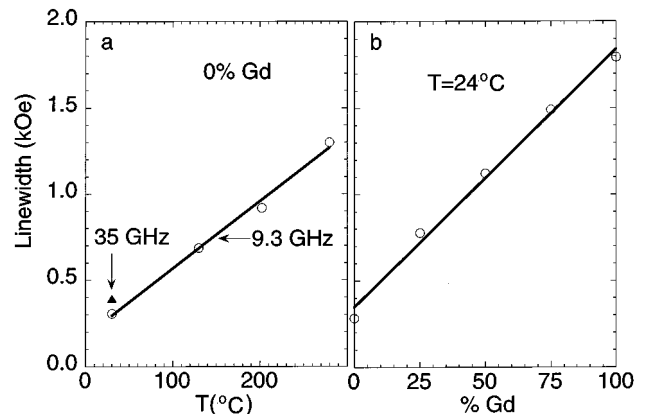


FIG. 5. (a) Peak-to-peak linewidth of bulk $\text{La}_{2/3}\text{Ca}_{1/3}\text{MnO}_3$ vs temperature at 9.3 GHz. (b) Peak-to-peak linewidth of bulk $(\text{La}_x\text{Gd}_{1-x})_{2/3}\text{Ca}_{1/3}\text{MnO}_3$ at room temperature vs Gd concentration.

tion. (2) The linewidth increases linearly with temperature. (3) The linewidth is nearly independent of frequency, increasing a bit from 9.3 to 35 GHz. (4) The g value is close to 2.0.

Searle and Wang performed electron spin resonance in the manganites.¹⁰ These authors examined the resonance line shape and linewidth of $\text{La}_{1-x}\text{Pb}_x\text{MnO}_3$ —a double-exchange ferromagnet with a maximum Curie temperature of 350 °C—in the temperature range from 77 to 430 K. In the ensuing years, several more studies have been reported.¹¹ The present study, however, differs from previous studies insofar as it investigates the effect of systematically substituting a moment-bearing rare-earth ion such as Gd for the $S=0$ La ion. We are thus able to supply some new information and ideas, even though we worked primarily with polycrystalline samples in the paramagnetic state.

It has long been established that the resonance linewidth of magnetic materials well above their ordering temperature can be exchange narrowed.¹² In the absence of strong exchange interactions, the linewidth of the paramagnet is caused by the random dipolar field experienced by each spin from all its neighboring spins. This field, denoted by ΔH_{dip} , is of order of magnitude M (the zero-temperature magnetization) and can be more precisely evaluated by the Van Vleck method of moments.¹³ The exchange energy produces mutual spin flips, which reduces the dipolar broadening. When the exchange interaction energy is large compared to the dipolar energy, the linewidth ΔH is given by the expression

$$\Delta H = \frac{(\Delta H_{\text{dip}})^2}{H_{\text{ex}}}, \quad (2)$$

where H_{ex} is the (suitably defined) exchange field, of order kT_c/μ_B . This equation assumes that the contribution of the spin-lattice relaxation to the linewidth can be neglected.

In $(\text{La}_{1-x}\text{Gd}_x)_{2/3}\text{Ca}_{1/3}\text{MnO}_3$ the dipolar field arises from *both* the Mn and Gd ions. However, the exchange field at the Mn site is roughly two orders of magnitude *larger* than the exchange field at the Gd sites. Thus the dipolar field is narrowed in $\text{La}_{2/3}\text{Ca}_{1/3}\text{MnO}_3$ (where $\Delta H=300$ Oe), but not in $\text{Gd}_{2/3}\text{Ca}_{1/3}\text{MnO}_3$ (where $\Delta H=2000$ Oe). We have found that manganites incorporating other rare-earth ions—even those with non- S -state ground states such as Nd—have linewidths of the same order of magnitude as $\text{Gd}_{2/3}\text{Ca}_{1/3}\text{MnO}_3$.

The observation that the linewidth is nearly independent of frequency (or, equivalently, applied magnetic field H) is (nearly) consistent with the exchange narrowing expression, Eq. (2), which predicts a linewidth with no dependence on the applied field. Of course, Eq. (2) is a limiting expression, strictly valid for $T \gg T_c$, and assumes negligible spin-lattice relaxation.

On the other hand, the temperature dependence of the linewidth is at odds with a purely exchange-narrowed line shape. The quasilinear increase of the linewidth with temperature indicates that an additional temperature-dependent spin-lattice contribution becomes evident at higher temperatures. At room temperature, this mechanism is apparently dominated by the exchange-narrowed spin-spin interaction discussed above. At higher temperatures the spin-lattice relaxation determines the linewidth. The linear temperature de-

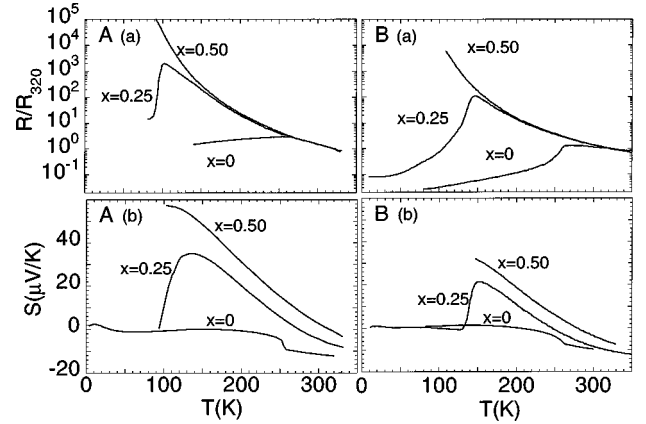


FIG. 6. (A) (a) Resistance (normalized) and (b) thermopower vs temperature for ceramic samples of $(\text{La}_{1-x}\text{Gd}_x)_{2/3}\text{Ca}_{1/3}\text{MnO}_3$, $x=0.0, 0.25$, and 0.50 . (B) (a) Resistivity (normalized) and (b) thermopower vs temperature for PLD thin film samples of $(\text{La}_{1-x}\text{Gd}_x)_{2/3}\text{Ca}_{1/3}\text{MnO}_3$, $x=0.0, 0.25$, and 0.50 at $H=0$.

pendence of the linewidth is not inconsistent with such an explanation. (The possibility that the exchange interaction decreases with temperature, causing an increase in linewidth, is not likely considering the magnitude of the effect. Several workers have previously observed similar temperature dependences in other exchange-narrowed materials¹⁴ and attributed them to a temperature-dependent exchange field.)

The resonance linewidth attains a *minimum* value near the Curie point. In the ferromagnetic state, it increases with decreasing temperature.¹⁵ In polycrystalline samples, this increase in linewidth is caused by the irregular shape of the crystallites and the resulting distribution of the demagnetizing factors. In single crystals or in thin films, the linewidth also increases with decreasing temperature below the ordering temperature. This result is thought to have its origin in an intrinsic granularity or inhomogeneity which seems to be present in most of these mixed valence manganite materials.¹⁶ The g value remains fixed at $g \cong 2$ in the ferromagnetic state. Oseroff *et al.*¹¹ have reported that the peak-to-peak linewidth of $\text{La}_{2/3}\text{Ca}_{1/3}\text{MnO}_3$ increases linearly with temperature from a minimum value of several hundred gauss at room temperature to a value of ~ 2 kOe at 800 °C, again suggesting that spin-lattice relaxation of the Mn ions is responsible for the high-temperature linewidth, while the room-temperature linewidth is determined by the exchange-narrowing mechanism.

V. TRANSPORT PROPERTIES (La-Gd)

In this section we briefly discuss the resistivity and thermopower in polycrystalline ceramic and pulsed laser deposition (PLD) film samples of composition $(\text{La}_{1-x}\text{Gd}_x)_{2/3}\text{Ca}_{1/3}\text{MnO}_3$. Many of these results have been previously reported in joint publications with the University of Illinois group led by Salamon.⁸ Figure 6(B) shows plots of (a) resistivity (normalized) and (b) thermopower for PLD films with $x=0, 0.25$, and 0.50 . These films were made from the identical ceramic material of Fig. 1 and were laser ablated and deposited on a LaAlO_3 substrate. The resistivity peak of the $x=0$ *thin film* is at 265 K and drops to 142 K at $x=0.25$. The resistivity peak of the $x=0$ *ceramic* sample,

TABLE I. Parameters used in Eq. (3) to fit thermopower and resistivity data of ceramic samples with the composition $(\text{La}_{1-x}\text{Gd}_x)_{2/3}\text{Ca}_{1/3}\text{MnO}_3$ for $x=0.0, 0.25, \text{ and } 0.50$.

Percent Gd	E_σ (eV)	E_S (eV)	S_∞ ($\mu\text{V}/\text{K}$)
0%	0.140	0.004	-23
25%	0.145	0.015	-54
50%	0.140	0.018	-56

from which this thin film was evaporated, is at 255 K and drops to 95 K for $x=0.25$. The resistance and thermopower results for the ceramic materials are displayed in Figs. 6(A), (a) and (b), respectively. Samples with $x \geq 0.5$ are insulators, as noted in Fig. 2, and do not display a resistivity peak. The properties of the thin film are found to differ somewhat from the target material. This effect can result from several causes during the film growth: epitaxial growth of the perovskite on the LaAlO_3 substrate, segregation of the La and Ca cations, or loss of oxygen.

In this section we shall *only* discuss the behavior of these samples in the insulating phase, at temperatures *above* the resistivity maximum. In later sections we shall extend the discussion to the entire temperature range. We assume, in accordance with current thought, that the conductivity in the high-temperature regime is dominated by the hopping motion of self-trapped small polarons.¹⁷ In this high-temperature regime, the classical expressions for the electrical resistivity ρ and the Seebeck coefficient for thermoelectricity, S , are given by the expressions⁸

$$\rho = \rho_0 T \exp\left(\frac{E_\sigma}{k_B T}\right), \quad (3)$$

$$S = \frac{k_B}{e} \left(\frac{E_S}{k_B T}\right) + S_\infty,$$

where E_σ and E_S are the (unequal) activation energies for the resistivity and the thermopower, respectively, and S_∞ is the Seebeck coefficient at asymptotically high temperatures—a measure of the entropy of crystalline and magnetic disorder. (Other symbols have their conventional meanings.) By fitting the experimental data to Eq. (3), we obtain the sets of parameters shown in Table I for the ceramic samples. Similar values are obtained for the PLD films. The large discrepancy between activation energy for conductivity, E_σ , and thermopower, E_S , is a hallmark of polaronic transport.¹⁷ Since the factor (k_B/e) of Eq. (3) determines the slope of the Seebeck coefficient at high temperatures (with the convention that e is negative for electrons), we conclude from the sign of E_σ that charge carriers are holelike in these three samples above the Curie temperature. The magnitude of S_∞ is not well understood, although Hundley and Neumeier¹⁸ have recently written on this subject.

What sort of things do we learn by measuring the transport properties of Gd-substituted samples? It is possible to learn something about the nature of the magnetic polarons. By comparing the (0% Gd)/(100% La) sample to the (25% Gd)/(75% La) sample, we find that substituted Gd ions lower the Mn-Mn exchange interaction substantially by bending the Mn-O-Mn bond angle.

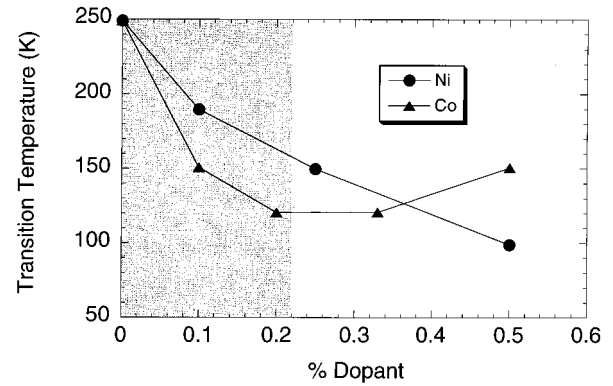


FIG. 7. Magnetic transition temperature vs dopant concentration for a series of bulk $\text{La}_{2/3}\text{Ca}_{1/3}(\text{Mn}_{1-x}\text{Co}_x)\text{O}_3$ and $\text{La}_{2/3}\text{Ca}_{1/3}(\text{Mn}_{1-x}\text{Ni}_x)\text{O}_3$ samples. Shaded portion represents region where samples are electrically conducting below the transition temperature. At concentrations where no ferromagnetic transitions are observed, the temperature of the irreversibility peak (Fig. 3) is used.

However, the polaron activation energy is changed very little by the substitution of Gd for La. Despite the large change in the exchange energy (as determined by their Curie temperatures), there is virtually *no* change in the activation energy for conduction E_σ (~ 140 meV). From this fact certain theories of polaron formation may be eliminated. For example, Dionne¹⁹ has proposed an interesting polaron theory in which the electrons become self-trapped at the Curie temperature, with an activation energy E_σ which is (nearly) equal to the exchange energy ($2zJ_{12}S_1S_2$, using conventional symbolism). Dionne's hypothesis does not appear to be tenable since it appears to conflict with our observations concerning Gd-La-substituted compounds where the Curie temperatures are observed to change without a corresponding change in the activation energies.

VI. COBALT AND NICKEL SUBSTITUTIONS

These samples were fabricated, as before, by grinding, pressing, and reacting the appropriate mixtures of oxides and carbonates. The samples were reacted under oxygen at a temperature of 1300 °C several times and then x rayed. The powder x-ray-diffraction spectra of $\text{La}_{2/3}\text{Ca}_{1/3}(\text{Mn}_x\text{Co}_{1-x})\text{O}_3$ and $\text{La}_{2/3}\text{Ca}_{1/3}(\text{Mn}_x\text{Ni}_{1-x})\text{O}_3$ are displayed in Fig. 1. The orthorhombically distorted single-phase perovskite structure is present in all the Co samples, but the Ni samples were found to be multiphase for Ni concentrations in excess of 75%. These samples, with 75% and 100% Ni, probably should have been sintered at a lower temperature in order to form the proper phase. We did not remake these samples, and we will only report on $\text{La}_{2/3}\text{Ca}_{1/3}(\text{Mn}_x\text{Ni}_{1-x})\text{O}_3$ with $1.0 \geq x \geq 0.50$. The literature⁷ indicates, however, that LaNiO_3 is a nonmagnetic Pauli paramagnet, and so we have reason to expect that $\text{La}_{2/3}\text{Ca}_{1/3}\text{NiO}_3$ will also be a Pauli paramagnetic metal.

The $\text{Mn}_{100}\text{Co}_0$, $\text{Mn}_{90}\text{Co}_{10}$, $\text{Mn}_{100}\text{Ni}_0$, $\text{Mn}_{90}\text{Ni}_{10}$, and $\text{Mn}_{75}\text{Ni}_{25}$ samples were ferromagnetic and have Curie points which are indicated in Fig. 7 for polycrystalline Mn-Co samples and for polycrystalline Mn-Ni samples. (In this notation, $\text{Mn}_{100}\text{Co}_0$ refers to the compound $\text{La}_{2/3}\text{Ca}_{1/3}\text{MnO}_3$.) The remaining samples displayed spin-glass behavior, in

which the field-cooled and zero-field-cooled traces diverged below the spin-glass temperature. The remaining samples are spin glasses. In Fig. 7 we have plotted the Curie or the spin-glass temperature as a function of Ni or Co doping. The shaded region of the plot represents the region of the phase diagram where the materials are found to exhibit metallic behavior at low temperatures. The metal-insulator transition nearly coincides with ferromagnetic-paramagnetic transition.

It is apparent from Fig. 7 that there is a large initial drop in the Curie temperature as a function of Co or Ni doping. There are two process which can contribute to this condition: (1) changes in the Mn-O-Mn bond angle which are caused by substituting a larger Ni or Co ion for a Mn ion, and (2) the inability of an itinerant electron to hop or tunnel, without assistance from a Mn ion to a neighboring Ni or Co ion.

First, we consider the effect of the Ni and Co ions on the Goldschmidt tolerance factor, defined in Eq. (1). Using the ionic radii tabulated by Shannon,²⁰ we find $t=0.916$, 0.927 , and 0.938 for $\text{La}_{2/3}\text{Ca}_{1/3}\text{MnO}_3$, $\text{La}_{2/3}\text{Ca}_{1/3}(\text{Mn}_{0.90}\text{Co}_{0.10})\text{O}_3$, and $\text{La}_{2/3}\text{Ca}_{1/3}(\text{Mn}_{0.90}\text{Ni}_{0.10})\text{O}_3$, respectively. (In this calculation, we used 6 as the coordination number for the 3+ and 4+ transition-metal ions and 9 as the coordination number for the La^{3+} and Ca^{2+} ions.) Using the phase diagram of Fig. 1, we find that the expected lattice contraction caused by substituting 10% Co or 10% Ni should have the effect of *increasing* the Curie temperature from 250 to 350 K. Since the Curie temperature is observed to substantially *decrease* under these circumstances, it is necessary to hypothesize another, more potent mechanism.

Since the Zener double-exchange mechanism is ineffective unless an electron can hop (or tunnel) between nearest-neighbor transition-metal ions without altering its spin or energy, we can attribute the lowering of the Curie point by Co (or Ni) substitutions to an assumed energy inequivalence of the ground-state energies of neighboring Mn and Co (or neighboring Mn and Ni) ions. We can estimate the magnitude of this effect by making some assumptions. We first assume that the low-temperature charge carriers are *band* polarons. Further, we assume that the differences between the binding energies of an electron on a Co (Ni) ion and Mn ion exceed the polaron bandwidth (which eliminates the possibility of energy-conserving coherent hops). Finally, as a result of these conditions, we can conclude that there is no double-exchange interaction between neighboring Co (Ni) ions and Mn ions. We can estimate that the change in the Curie temperature ΔT_c is related to the concentration of impurity ions, c , by the approximate relationship

$$\frac{\Delta T_c}{T'_c} \approx -c. \quad (4)$$

Here, T'_c is the Curie temperature in the absence of the antiferromagnetic superexchange interaction, the latter obtained from the Néel temperature of LaMnO_3 , $T_N=50$ K. Hence $\Delta T_c \approx -300c$, and a 10% impurity concentration is estimated to yield a decrease of 30 K in the magnetic transition temperature. This is the correct sign and order of magnitude for the drop in the transition temperatures of $\text{La}_{2/3}\text{Ca}_{1/3}(\text{Mn}_{0.90}\text{Co}_{0.10})\text{O}_3$ and $\text{La}_{2/3}\text{Ca}_{1/3}(\text{Mn}_{0.90}\text{Ni}_{0.10})\text{O}_3$.

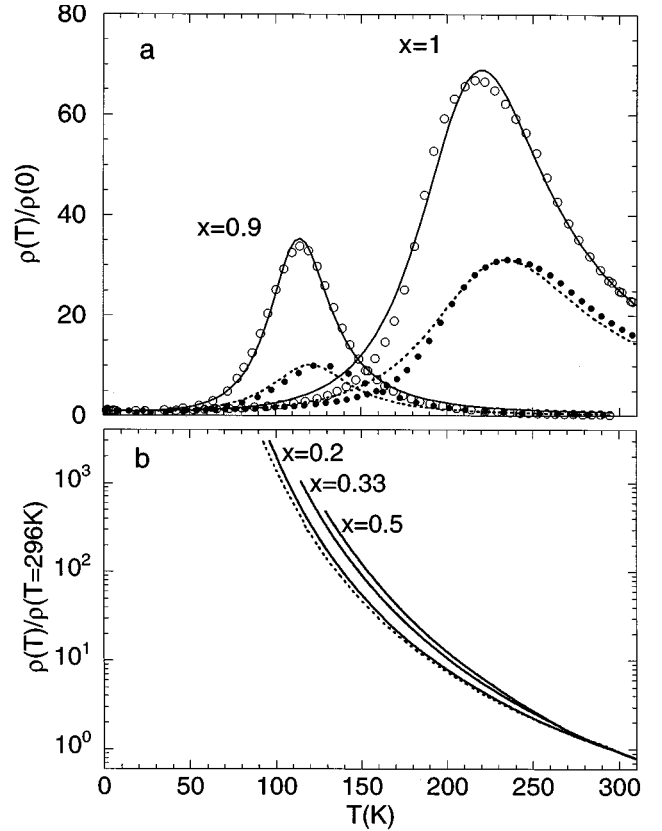


FIG. 8. Temperature dependence of electrical resistance of a series of $\text{La}_{2/3}\text{Ca}_{1/3}(\text{Mn}_x\text{Co}_{1-x})\text{O}_3$ laser-ablated thin films. (a) A least-squares fit of Eq. (5) to the electrical conductivity data of two CMR compounds $\text{La}_{2/3}\text{Ca}_{1/3}(\text{Mn}_x\text{Co}_{1-x})\text{O}_3$ with a resistivity maximum $x=1.0$ and 0.9 . The symbols are representative data points, and the lines are the fits to the data. The open circles show the data at $H=0$, and the solid lines are the results from a fit to this data. The solid circles show the data at $H=2.5$ T, and the dashed lines are the results from fit to the data. The resulting fitting parameters are given in Table II. Shown in (b) is the electric resistivity data of three CMR compounds $\text{La}_{2/3}\text{Ca}_{1/3}(\text{Mn}_x\text{Co}_{1-x})\text{O}_3$ with $x=0.2$, 0.33 , and 0.5 , which are insulators at all temperatures. The dashed line is the resistivity of the $x=0.2$ compound at $H=2.5$ T.

VII. RESISTIVITY (Co-Mn AND Ni-Mn)

In Figs. 8(a) and 8(b), the temperature dependence of electrical *resistance* of a series of $\text{La}_{2/3}\text{Ca}_{1/3}(\text{Mn}_x\text{Co}_{1-x})\text{O}_3$ laser-ablated *thin films* is displayed. Figure 8(a) displays a least-squares fit of Eq. (5) (to be discussed below) to the electrical conductivity data of two CMR compounds $\text{La}_{2/3}\text{Ca}_{1/3}(\text{Mn}_x\text{Co}_{1-x})\text{O}_3$ with $x=1.0$ and 0.9 . The symbols are representative data points, and the lines are the fits to the data. The open circles show the data at $H=0$, and the solid lines are the results from fits to these data. The darkened circles show the data at $H=2.5$ T and the dashed lines are the results from a fit to the data. Shown in Fig. 8(b) is the electrical conductivity (data only) of three CMR compounds $\text{La}_{2/3}\text{Ca}_{1/3}(\text{Mn}_x\text{Co}_{1-x})\text{O}_3$ with $x=0.2$, 0.33 , and 0.5 , which evince only semiconducting temperature dependence. Where the resistivity maximum exists, it is close to a ferromagnetic transition temperature and is accompanied by a negative magnetoresistance.

We find it convenient to discuss our data in terms of

Zhang's spin-polaron theory.²¹ Zhang has adapted Holstein's classic lattice-polaron theory²² to the discussion of electrons which are self-trapped by the electron-magnon interaction. This theory, although less detailed and sophisticated than some others,²³ is elegant and physically transparent. We find it useful because its central result is a simple mathematical formula which can be easily used in conjunction with commercial curve-fitting computer programs.

Zhang's theory of electrical conductivity in perovskite structures is based on a Hamiltonian composed of only three terms: a single-electron kinetic energy term, a single-magnon energy term of the localized spins, and a term describing the Hund's-rule interaction between the itinerant electrons and localized spins. It omits complications resulting from magnon-magnon interactions, electron-electron interactions, and electron-phonon interactions. Using an approximation of a single optical magnon frequency ω_0 —a drastic assumption, especially at low temperatures—Zhang obtains the following expression for the conductivity at finite temperatures T and a finite applied field H :

$$\begin{aligned} \frac{\rho(0)}{\rho(T)} &= \frac{\sigma(T)}{\sigma(0)} \\ &= \exp\left[-\frac{2E_\sigma}{\omega_0} N(\omega_0 + g\mu_B S_c H)\right] \\ &\quad + \frac{b^2}{E_\sigma k_B T} \exp\left[\frac{-E_\sigma}{k_B T}\right]. \end{aligned} \quad (5)$$

In this equation, $N(\omega_0) = [\exp(\omega_0/k_B T) - 1]^{-1}$, the number of thermal magnons, E_σ is the activation energy of the (localized) spin polarons, and ω_0 and b are functions of the basic Hamiltonian, but we treat them here as adjustable parameters. This expression, which represents the sum of two parallel currents, has the following simple interpretation: The first term describes the coherent, elastic hopping of a spin polaron which is dominant at low temperatures, while the second term describes the incoherent, inelastic hopping dominant at high temperatures. These two conduction processes have very different temperature dependences. The former term describes band polarons with a temperature-dependent effective mass, whose conductivity *decreases* as the temperature increases; the latter describes thermally assisted hopping where the conductivity *increases* with increasing temperature. These two processes compete to yield the metal-insulator transition observed in the manganites. In our treatment of the transport properties of La-Gd perovskites, Sec. V, we only discussed the high-temperature behavior. In this section describing the Mn-Co and Mn-Ni perovskites, we attempt to expand this discussion to include the entire temperature range.

Equation (5) predicts that the resistivity decreases nearly exponentially with inverse temperature at high temperatures and increases linearly with temperature at low temperature. The former prediction is one of small-polaron hopping, which we have already utilized in our discussion of the high-temperature resistivity of $(\text{La}_{1-x}\text{Gd}_x)_{2/3}\text{Ca}_{1/3}\text{MnO}_3$. The low-temperature prediction will not be reflected in the data, since it requires knowledge of the magnon dispersion relationship—which is explicitly ignored in Zhang's calcula-

TABLE II. Parameters used in Eq. (8) to fit the resistivity data of PLD thin films with the composition $\text{La}_{2/3}\text{Ca}_{1/3}(\text{Mn}_{1-x}\text{Co}_x)\text{O}_3$ for $x = 0, 0.1, 0.2, 0.33, \text{ and } 0.5$.

Percent Co	E_σ (eV)	ω_0 (K)	b (eV)	S_c
0%	0.18	337	0.30	3.4
10%	0.09	159	0.32	8.7
20%	0.09			
33%	0.11			
50%	0.10			

tion. The true value of this equation is its simplicity and the reassurance that it is derived (with approximations) from a basic Hamiltonian.

Several purely *empirical* relations for the conductivity utilizing two parallel conducting channels have been previously proposed for the manganites²⁴ in which the low-temperature term is explicitly dependent on the magnetization, thereby forcing the resistivity maximum to coincide with the ferromagnetic transition temperature. Perhaps this can also be achieved using Eq. (5) by renormalizing the magnon frequency in a mean-field approximation so that $\omega_0 \rightarrow \omega_0[M(T)/M(0)]$. However, Zhang has informed us that he does not believe this is a proper procedure.²⁵ Questions relating to the proximity of the metal-insulator transition and the ferromagnetic-paramagnetic transition can be answered by rederiving the analog of Eq. (5), but keeping the magnon-magnon interactions in the basic Hamiltonian.

The solid lines and dashed lines of Fig. 8(a) are a plot showing the “best fit” of Eq. (5) to the conductivity data of two CMR compounds which display the resistivity maximum: $\text{La}_{2/3}\text{Ca}_{1/3}(\text{Mn}_x\text{Co}_{1-x})\text{O}_3$ with $x = 1.0$ and 0.9 . The other curves are from insulating compositions that do not show a resistivity maximum. The resulting fitting parameters are given in Table II.

We should not expect a highly accurate fit to the data for reasons which were outlined above (such as the neglect of dispersion and of electron-phonon interactions). But to us it seems to contain much of the right physics. The parameter E_σ is the polaron hopping energy, and all the samples fit the theory with physically acceptable values $E_\sigma \approx 100$ – 200 meV. Moreover, the “optical” magnon frequency ω_0 is found to scale, approximately, with the magnetic transition temperature T_c —another physically reasonable result. The value of the spin S_c used to fit the magnetic field dependence does not represent a single spin. It represents the value of a small cluster of spins—a phenomenon which has been previously noted by several authors. The large spins may come from a clustering of Ca ions or even of a nonuniform distribution of oxygens.

VIII. THERMOPOWER (Mn-Co AND Mn-Ni)

The ratio between the temperature differential and voltage across a sample is called the Seebeck coefficient S and is an intrinsic property of the material. The theory of this coefficient shows that it is a simple measure of the entropy per charge carrier (provided that electrons, not phonons, are the carriers of the heat energy).²⁶ At *low* temperatures, in a degenerate metal which may consist of band polarons, the See-

TABLE III. Parameters used in Eq. (8) [or Eq. (5)] for fitting the resistivity and thermopower data of bulk, sintered compositions $\text{La}_{2/3}\text{Ca}_{1/3}(\text{Mn}_{1-x}\text{Co}_x)\text{O}_3$ ($x=0$ and 0.1) and $\text{La}_{2/3}\text{Ca}_{1/3}(\text{Mn}_{1-x}\text{Ni}_x)\text{O}_3$ ($x=0.1, 0.25$, and 0.5).

Sample	E_S (eV)	E_σ (eV)	S_∞ ($\mu\text{V}/\text{K}$)	E_F (eV)	ω_0 (K)	b (eV)
Mn ₁₀₀	0.0028	0.2	-10	0.35	425	0.24
Mn ₉₀ Co ₁₀	0.0073	0.17	-34	0.24	274	4.7
Mn ₉₀ Ni ₁₀	0.0078	0.19	-28		314	5.2
Mn ₇₅ Ni ₂₅		0.13				
Mn ₅₀ Ni ₅₀		0.18				

beck coefficient is proportional to the first power of temperature and has the same sign as the charge carriers,

$$S \approx \frac{k}{e} \left[\frac{\pi^2}{3} \right] \left[\frac{k_B T}{E_F} \right]. \quad (6)$$

At *high* temperatures where the polarons are self-trapped and conduct electricity and heat by a thermal activation process, the Seebeck coefficient is inversely proportional to the temperature and is given by the formula already given in Eq. (3).

When two different kinds of carriers are present, each with a well-defined Seebeck coefficient S and conductivity σ , the measured thermopower is given by

$$S = (\sigma_1 S_1 + \sigma_2 S_2) / (\sigma_1 + \sigma_2). \quad (7)$$

Zhang has not published an equivalent formula to Eq. (5) for the Seebeck coefficient of a system of magnetic polarons. In its absence, we shall approximate the answer by using Eq. (7) with the partial conductivities taken from Eq. (5) and the partial Seebeck coefficients taken from Eqs. (6) and (3):

$$S(T) = \frac{AT \exp[-2E_\sigma/\omega_0]N(\omega_0) + (E_S/T + S_\infty) \frac{b^2}{E_\rho k_B T} \exp[-E_\sigma/k_B T]}{\exp[-2E_\sigma/\omega_0]N(\omega_0) + \frac{b^2}{E_\sigma k_B T} \exp[-E_\sigma/k_B T]}, \quad (8)$$

where we treat A , E_S , and S_∞ as parameters to be determined by fitting the data to the expression. The remaining parameters were obtained by fitting the measured resistivities to Eq. (5). The dependence of this expression on magnetic field is omitted, but appears in a similar fashion to Eq. (5). This equation predicts that the thermopower is zero at $T=0$ and initially increases (or decreases) linearly with temperature. At high temperatures, the thermopower is expected to decrease (increase) inversely proportional to temperature, attaining a value S_∞ at asymptotically high temperatures.

A least-squares fit of Eq. (8) to the zero-magnetic-field thermopower data of the sintered bulk compounds $\text{La}_{2/3}\text{Ca}_{1/3}(\text{Mn}_{90}\text{Co}_{10})\text{O}_3$ and $\text{La}_{2/3}\text{Ca}_{1/3}(\text{Mn}_{90}\text{Ni}_{10})\text{O}_3$ is shown in Fig. 9(a). The resistivity data for these compounds are shown in Fig. 9(b). The circles are representative data points, and the lines are the fits to the data. The resulting fitting parameters for the conductivity data for the compounds containing 10% Co and the compound containing 10% Ni, as well as those for other compositions, are tabulated in Table III. These parameters were held fixed in the fit of the data to Eq. (8). This conductivity data yielded the fitting parameters to the thermopower data, which are also displayed in Table III.

An omnipresent ‘‘bump’’ is present in the low-temperature thermopower of the lanthanum manganites at

≈ 20 K, and is probably not to be expected from any model which considers electronic contributions exclusively. This feature has previously been attributed to such mechanisms as ‘‘phonon drag’’ or ‘‘two-level systems,’’²⁷ but there appears to be no consensus. In the present paper, we shall simply ignore this feature. In addition, since the thermopower data become increasingly unreliable for samples of large resistivity, we shall only consider two samples: (a) 90% Mn 10% Co and (b) 90% Mn 10% Ni. (The 100% Mn sample is discussed in Ref. 8 and in several additional papers on thermopower in manganites.)

The Seebeck coefficient of the sample containing 100% Mn is zero at $T=0$. As the temperature increases, the sign of S oscillates about zero and then drops to $-8 \mu\text{V}/\text{K}$ at ≈ 250 K (the Curie temperature). From 250 to 350 K, S remains negative and declines steadily.

The Seebeck coefficient of sample (a), $\text{Mn}_{90}\text{Co}_{10}$, is zero at $T=0$ and then decreases with temperature quasilinearly. At the Curie temperature, 150 K, S abruptly begins to rise to a value of $+6 \mu\text{V}/\text{K}$. Above 180 K, $S(T)$ decreases inversely with temperature.

The Seebeck coefficient of sample (b), $\text{Mn}_{90}\text{Ni}_{10}$, remains very close to a value of zero in the temperature interval $0 < T < T_c$, where T_c is the Curie temperature of this material,

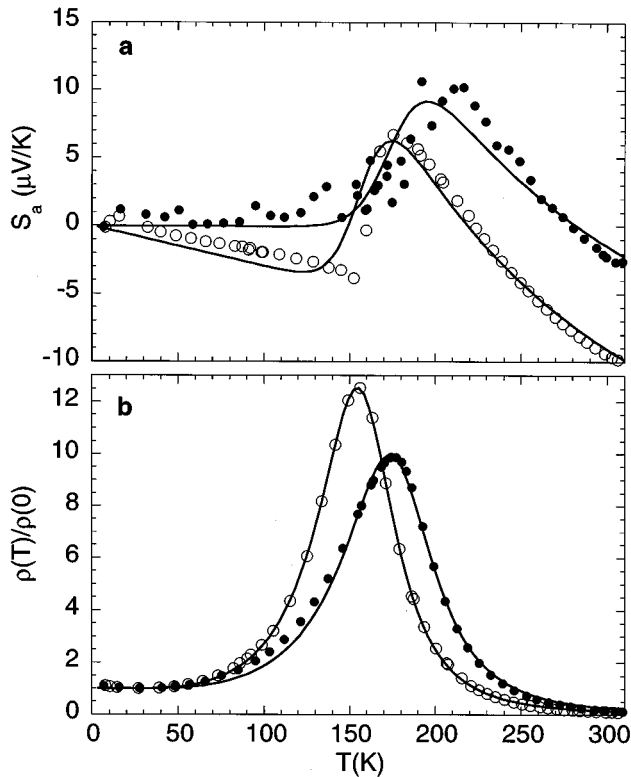


FIG. 9. (a) A least-squares fit of Eq. (8) to the thermopower data of the compounds $\text{La}_{2/3}\text{Ca}_{1/3}(\text{Mn}_{90}\text{Co}_{10})\text{O}_3$ (open circles) and $\text{La}_{2/3}\text{Ca}_{1/3}(\text{Mn}_{90}\text{Ni}_{10})\text{O}_3$ (solid circles). The symbols are representative data points and the lines are the fits to the data. (b) A least-squares fit of Eq. (5) to the electrical conductivity data of these compounds. The resulting fitting parameters for both the thermopower data and the conductivity data are given in Table III.

170 K. $S(T)$ then abruptly rises to a value $+15 \mu\text{V/K}$ at 200 K; at higher temperatures, it decreases with temperature in an inverse manner.

Above the Curie temperature, we find that the thermopower activation energy (binding energy) E_S equals 8 meV for both $\text{La}_{2/3}\text{Ca}_{1/3}(\text{Mn}_{0.90}\text{Co}_{0.10})\text{O}_3$ and $\text{La}_{2/3}\text{Ca}_{1/3}(\text{Mn}_{0.90}\text{Ni}_{0.10})\text{O}_3$ compared to 10 meV for $\text{La}_{2/3}\text{Ca}_{1/3}\text{MnO}_3$. At low temperatures, the initial sign of the Seebeck coefficient is positive for $\text{La}_{2/3}\text{Ca}_{1/3}\text{MnO}_3$, zero for $\text{La}_{2/3}\text{Ca}_{1/3}(\text{Mn}_{0.90}\text{Ni}_{0.10})\text{O}_3$, and negative for $\text{La}_{2/3}\text{Ca}_{1/3}(\text{Mn}_{0.90}\text{Co}_{0.10})\text{O}_3$.

The observation of oscillations in the sign of the thermopower is an indication that the low-temperature, narrow polaron bands may possess a complex density of states—one which can be altered by temperature. For example, Asamitsu *et al.*²⁸ have suggested that the double degeneracy of the e_g band can be split by temperature-dependent structural distortions, thereby altering the band filling factor between electrons and holes.

IX. PARAMAGNETIC RESONANCE (Mn-Co AND Mn-Ni)

In Fig. 10 we show the room-temperature 9.3-GHz EPR spectra of (a) $\text{La}_{2/3}\text{Ca}_{1/3}(\text{Mn}_{1-x}\text{Co}_x)\text{O}_3$ and (b) $\text{La}_{2/3}\text{Ca}_{1/3}(\text{Mn}_{1-x}\text{Ni}_x)\text{O}_3$ for some representative values of x . These resonances are all observed *above* the Curie temperature. The asymmetry of the $\text{La}_{2/3}\text{Ca}_{1/3}(\text{Mn}_{1-x}\text{Ni}_x)\text{O}_3$ line

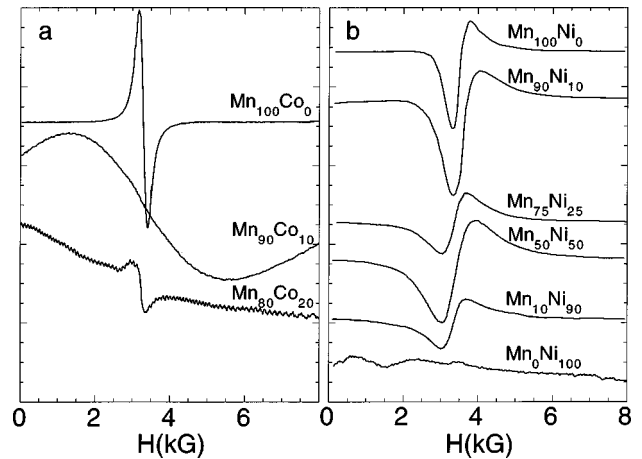


FIG. 10. Room-temperature 9.3-GHz EPR spectra of sintered ceramic samples of (a) $\text{La}_{2/3}\text{Ca}_{1/3}(\text{Mn}_{1-x}\text{Co}_x)\text{O}_3$ and (b) $\text{La}_{2/3}\text{Ca}_{1/3}(\text{Mn}_{1-x}\text{Ni}_x)\text{O}_3$. The asymmetric line shape results from the effects of electrical conductivity. The weak, narrow $g=2$ resonance in the $\text{Mn}_{80}\text{Co}_{20}$ spectrum is probably caused by a weak second phase. The $\text{Mn}_0\text{Ni}_{100}$ is multiple phase, but the weak resonances from this sample originate in the empty microwave cavity.

shapes is caused by skin depth complications due to the use of sintered, bulk, conducting samples. A loose powder sample was used in studying the spectra of $\text{La}_{2/3}\text{Ca}_{1/3}(\text{Mn}_{1-x}\text{Co}_x)\text{O}_3$. In these figures, only the line shapes are meaningful; the intensities may bear little relation to one another as the spectrometer sensitivity was altered from run to run.

The effects of Co and Ni substitutions on the $\text{La}_{2/3}\text{Ca}_{1/3}\text{MnO}_3$ resonance spectra differ markedly from one another. On the one hand, Co substitutions drastically broaden the resonance line. At room temperature, polycrystalline $\text{La}_{2/3}\text{Ca}_{1/3}\text{MnO}_3$ has a linewidth of 350 Oe. When Co atoms are substituted for 10% of the Mn atoms, the linewidth increases to 4000 Oe. When Co atoms are substituted for 20% of the Mn atoms, the resonance is incompletely visible on a 10 000 Oe sweep; we estimate the linewidth of the $\text{Mn}_{80}\text{Co}_{20}$ sample to be approximately 10 000 Oe. The weak, narrow resonance in the center of the $\text{Mn}_{80}\text{Co}_{20}$ spectrum is attributed to a weak, second phase of the sample. On the other hand, the effect of Ni is to progressively *weaken* the resonance without *broadening* it substantially. In Fig. 11 we plot the linewidths of Co-doped and Ni-doped manganites as a function of dopant concentration. We see that the linewidth of the cobalt-substituted samples increases strongly with cobalt concentration, while the linewidth of the nickel-substituted samples is nearly independent of Ni concentration.

We have previously discussed the broadening effect of Gd on the manganite paramagnetic resonance in Sec. IV, where we surmised that the broadening near room temperature was primarily caused by the dipolar field of the Gd ions. However, the origin of line broadening in Co- and Ni-substituted manganites is more complex. The Co and Ni ions weaken the exchange field, as determined by the reduction in the Curie temperature, but this is too small an effect, in itself, to account for the large increase in the linewidth of Co-substituted compounds. It seems reasonable to conclude that Co ions broaden the paramagnetic resonance line by a rapid spin-

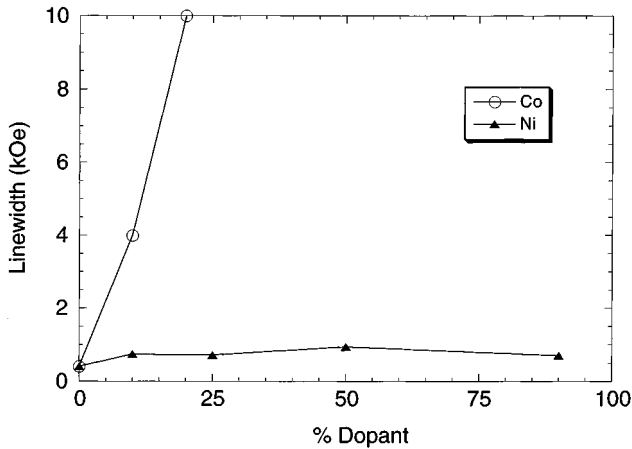


FIG. 11. Dependence of the linewidth on dopant concentration for $\text{La}_{2/3}\text{Ca}_{1/3}(\text{Mn}_{1-x}\text{Co}_x)\text{O}_3$ (open circles) and $\text{La}_{2/3}\text{Ca}_{1/3}(\text{Mn}_{1-x}\text{Ni}_x)\text{O}_3$ (dark triangles).

lattice relaxation of the Co ion. Accordingly, we attribute the insensitivity of the linewidth to Ni doping to a smaller spin-lattice relaxation mechanism for the Ni ion.

An alternative explanation for the disparate behaviors of the Ni- and Co-substituted samples is the “bottleneck” effect²⁹ which can develop between the Mn and Ni spin systems when both ions g values are close to 2.0. Another possibility may be that the Mn/Ni samples are segregated into Ni-rich and Ni-poor regions.

X. DISCUSSION

In the preceding sections of this paper, we have presented the results of a variety of disparate experiments on cobalt-, nickel-, and gadolinium-substituted $\text{La}_{2/3}\text{Ca}_{1/3}\text{MnO}_3$ compounds. In this section, we shall attempt to provide a short discussion of each of the following points: (a) the connection of the EPR results to the transport properties, (b) the relationship between the experiments on bulk materials and thin films, and (c) the systematic variation, if any, of the spin-polaron-model parameters.

A. Relationship of EPR data to transport measurements

We have already established that substitution by Gd^{3+} ions of La^{3+} ions influences the magnetic and transport properties primarily by distorting the lattice due to the disparity between the Gd^{3+} and La^{3+} ionic radii. These distortions, evident in powder x rays, Fig. 1, serve to alter the Mn-O-Mn bonding angles and modify both the exchange and transfer integrals, whose values determine the magnetic and electrical properties.

The effect of Gd substitution on the EPR spectra is also strong (Figs. 4 and 5). We have attributed the increased linewidth of the Gd-doped specimens to the (non-exchange-narrowed) dipolar fields originating at the Gd^{3+} spin moment. The transport and EPR, results are indeed consistent with one another. Despite the substantial influence of the Gd ion on both the transport and resonance parameters, neither phenomenon requires anything but passive involvement from the rare-earth ion, whose electrons remain unhybridized with the conduction electrons and stay localized about their rare-earth core.

We have previously inferred that the effect of replacing a Mn ion with a transition-metal ion such as Ni or Co, in $\text{La}_{2/3}\text{Ca}_{1/3}\text{MnO}_3$, is not at all the same as the replacement of La^{3+} by Gd^{3+} . Both the transition-metal replacements and the rare-earth replacements lower the magnetic and metal-insulator transition temperatures, but they do so by completely different physical mechanisms. While Gd lowers the transition temperature by distorting the lattice, Ni and Co have little effect on the lattice. These transition-metal ions decrease the Curie temperature by forbidding the energy- and spin-conserving double-exchange event between it and its nearest-neighbor Mn ions. This process is allowed only between two ions of identical (to within a bandwidth) ground-state energies, with each ion possessing a very large Hund’s-rule interaction energy.

EPR studies can relate to the magnetic and transport investigations by identifying the ground states of the individual transition-metal ions. The optimal, unalloyed compound $\text{La}_{2/3}\text{Ca}_{1/3}\text{MnO}_3$ has a relatively narrow $g=2.0$ resonance, indicating a very small admixture of orbital angular momentum in the ground state. Replacing the Mn ions with either Co or Ni ions in the pure Mn oxide also produces compounds with a $g=2.0$ resonance. However, the effect of substituting Co ions on EPR spectra is to significantly increase the linewidth to the point where the resonance cannot be observed observable at 20% Co. The effect of substituting Ni ions for Mn ion is dramatically different, since the linewidth remains almost unchanged with the addition of Ni (Figs. 10 and 11). Similar effects have been observed in many other alloy families—e.g., $3d$ impurities in metals or in exchange-coupled paramagnets—and have been satisfactorily explained by the phenomenon of “bottlenecking.”³⁰

The bottleneck effect occurs when the “host” and “impurity” resonances have similar g values and the spin-lattice relaxation rate of the impurity spin is sufficiently small. If these conditions are met, the two spin systems couple to each other, producing a narrow resonance line. Otherwise, with no bottleneck, the impurity can rapidly relax the host resonance, resulting in a very broad resonance line. Using the criteria for bottlenecking, we deduce that Ni impurities in $\text{La}_{2/3}\text{Ca}_{1/3}\text{MnO}_3$ have $g \cong 2.0$; contrariwise, Co impurities in $\text{La}_{2/3}\text{Ca}_{1/3}\text{MnO}_3$ have a g value far from 2.0.

The possible ionization states for the Ni and Co impurities in $\text{La}_{2/3}\text{Ca}_{1/3}\text{MnO}_3$ are 3^+ , 4^+ , and (in the case of dissociation) 2^+ . Since the Ni ions are assumed to participate in the bottleneck process, a *sine qua non* is that these ions have a g value near 2.0 and that they have a small spin-lattice relaxation. This combination implies that the orbital angular momentum is quenched, $\langle L \rangle = 0$ to first order. The electrons must then completely fill an “octahedral subshell” to accomplish this. Of the three possible nickel ionization states, only Ni^{2+} —a (d^8) configuration—fills the bill. Co, on the other hand, is known to exist both in the high- and low-spin configurations and the Co^{3+} and Co^{4+} ionization states. It cannot act as a bottleneck, and its broadening effect on the Mn resonance is understandable.

B. Bulk samples vs thin films

Some experiments, such as Hall effect and ferromagnetic resonance, can only be performed on thin films, whereas

other experiments can be performed on thin films and bulk samples. In prior sections we have referred to data from bulk samples and from thin films of the same nominal composition. In Figs. 6(A) and 6(B) we have compared and contrasted the electrical resistance and thermopower of both forms of $(\text{La}_{1-x}\text{Gd}_x)_{2/3}\text{Ca}_{1/3}\text{MnO}_3$ samples. Since the measured parameters of the bulk samples and their corresponding thin films disagree, the question concerning the origin of these differences naturally arises.

Ever since the earliest report of colossal magnetoresistance,³¹ it has been evident that the properties of thin films and those of bulk samples (or those thin films annealed at elevated temperatures under oxygen) were somewhat different. Since then, several experimental papers have reported on the variability of manganite properties with oxygen content. (Perhaps the most dramatic evidence of this phenomenon is the conversion of LaMnO_3 from an antiferromagnet to a ferromagnet precipitated by a slight increase in the oxygen content.) Since the parameters of thin films can often be optimized by annealing them in an oxygen-rich atmosphere, we feel that the major source of variation between the thin film and bulk properties is primarily caused by a corresponding variation in the oxygen content.

A similar variability exists in the properties of bulk samples whenever the oxygen content is not carefully controlled. As mentioned earlier in the text, we have attempted to optimize the oxygen content by sintering and annealing each sample under identical conditions. We have *not* verified the oxygen content by chemical or physical measurements, but where possible, we have confirmed that our results are in agreement with previously published measurements.

C. Spin-polaron model

Numerous parameters are found in Zhang's spin-polaron theory. Four parameters are contained in the expression for the conductivity, Eq. (5): E_σ , ω_0 , b , and S_c . Three additional parameters are contained in the thermopower expression of Eq. (8): A , E_S , and S_∞ .

At temperatures high with respect to the resistivity-peak temperature, Zhang's model becomes identical with the theory of small adiabatic polarons, and the two surviving parameters E_S and S_c are identified with the polaron activation energy (which is approximately equal to half the polaron binding energy) and with the spin of the core electrons, respectively. (This small-polaron theory, with matrix elements modified by the Jahn-Teller distortion, is currently in favor with some experimentalists and theorists.²³) Had we been able to extend our conductivity measurements to higher temperatures, our values for these parameters would, doubtless, prove to be more accurate. In the case of pure $\text{La}_{2/3}\text{Ca}_{1/3}\text{MnO}_3$, where others have used small-polaron theory to describe their own high-temperature data, we may justify our use of Zhang's theory by comparing our own parameters to those obtained by previous workers. Jaime *et al.*⁸ obtained $E_S = 126$ meV and Tanaka *et al.*³² report $E_S = 116$ meV for a $\text{La}_{0.8}\text{Ca}_{0.2}\text{MnO}_3$ sample, while we have obtained values of E_S which vary between 130 and 140 meV (for different samples) by fitting Zhang's theory to data obtained below 300 K.

The remaining parameter S_c is the value of the "core" spin. It is greatly in excess of the $S=2$ value which we

expect from Mn^{4+} spins. This effect has previously been observed in many samples displaying colossal magnetoresistance. Several explanations have been offered, some involving granular superparamagnetism and others involving a spin bottleneck between Mn^{3+} and Mn^{4+} ions. No generally accepted explanation exists, as of yet.

The equation which we have utilized for fitting our thermopower data, Eq. (8), reduces to the standard expression obtained for small-polaron hopping at sufficiently high temperatures and yields value of E_S in reasonable agreement with existing data in the case of $\text{La}_{2/3}\text{Ca}_{1/3}\text{MnO}_3$. (There appears to be little agreement for the value of the Seebeck coefficient at "infinite" temperature, S_∞ , from experiment or from theory.)

Finally, we arrive at the discussion of the low-temperature parameters of the equations. The most illuminating aspect of Zhang's theory is that it does not demand the existence of an abrupt metal-insulator transition. Instead, the theory posits the existence of two coexisting electronic processes: a coherent, energy-conserving tunneling process and an incoherent, thermally assisted hopping process. Both processes are temperature dependent, with the probability of the former decreasing with temperature, while the probability of the hopping process increases with temperature. At some intermediate temperature near the peak in the temperature-dependent resistivity, the hopping process will overwhelm the tunneling process, and the sample appear to behave as an insulator at higher temperatures. Zhang points out that the peak temperature need not coincide with the Curie temperature—and indeed, many workers have reported that the two temperatures are not identical. However, the Curie temperature and the resistivity-peak temperature are not independent, since they both depend on the number of thermal magnons. Zhang's treatment, which we have used, exacerbates this discrepancy by failing to include the magnon-magnon interaction in the Hamiltonian, which, in turn, causes the average magnetization to diminish with temperature in a critical fashion. Including this interaction in the theory, even in a crude mean-field fashion, will undoubtedly have the effect of bringing the "metal-insulator" temperature and the Curie temperature closer together.

XI. CONCLUSIONS

We have examined the experimental consequences of some elemental replacements within the colossal magnetoresistive compound $\text{La}_{2/3}\text{Ca}_{1/3}\text{MnO}_3$. First, we have systematically replaced the La ions with Gd ions and investigated the resulting changes in the paramagnetic resonance linewidth and magnetic transition temperature. We have concluded that the paramagnetic resonance linewidth at room temperature is primarily caused by exchange-narrowed Mn dipolar fields, while Gd dipolar fields are largely unaffected by the exchange process. At higher temperatures another process, presumably spin-lattice relaxation, begins to dominate the paramagnetic linewidth, causing the linewidth to increase linearly with temperature.

The phase diagram, constructed by plotting the magnetic transition temperature of $(\text{La}_{1-x}\text{Gd}_x)_{2/3}\text{Ca}_{1/3}\text{MnO}_3$ versus the average rare-earth ionic radius (or, equivalently, the tolerance factor t), agrees very well with phase diagrams of

other rare-earth manganites found by other workers. From this, we have concluded that the magnetic transition of $(\text{La}_{1-x}\text{Gd}_x)_{2/3}\text{Ca}_{1/3}\text{MnO}_3$ is determined, primarily, by a size effect, namely, the *average* ionic radius of the rare-earth ion.

The effects of replacing the Mn ions in $\text{La}_{2/3}\text{Ca}_{1/3}\text{MnO}_3$ by Co and Ni ions were also investigated. The effects of this replacement on the magnetic transition temperature are strong, but are *not* caused by an ion size effect. Instead, we have postulated that the observed reduction of the Curie temperature with Mn substitution is caused by the absence of double exchange interactions between unlike transition ions.

The effect of Co and Ni substitutions on the electrical resistivity and thermopower was presented and parametrized with Zhang's magnetic polaron theory. While Zhang's treatment yields a good qualitative fit to the data with and without an applied magnetic field, more work is needed to yield a

good quantitative fit. Finally, the effects of Ni and Co substitutions on the paramagnetic linewidth were displayed, and the Ni ion was found to be a Ni^{2+} ion.

ACKNOWLEDGMENTS

We wish to thank Professor S. F. Zhang for providing clarifications on his paper. Many of the measurements and interpretations of the La-Gd transport properties were done by Marcelo Jaime and Myron Salamon. The authors thank them for a fruitful collaboration. The authors are grateful to Dr. Krystl Hathaway for her careful reading of this manuscript. Recently, we were informed of complementary work by Ahn *et al.*³³ on the properties of Fe-substituted manganites.

- ¹J. M. Tarascom, L. H. Greene, W. R. McKinnon, and G. W. Hall, *Phys. Rev. B* **35**, 1373 (1987).
- ²G. Xiao, F. H. Streitz, A. Garvin, Y. W. Du, and C. L. Chien, *Phys. Rev. B* **35**, 1373 (1987).
- ³Paul Grant, *New Sci.* **30**, 36 (1987).
- ⁴Helen D. Megaw, *Proc. Phys. Soc. London* **58**, 133 (1946).
- ⁵C. Zener, *Phys. Rev.* **82**, 403 (1951).
- ⁶G. Briceno, H. Chang, X. Sun, P. Schultz, and X. D. Xiang, *Science* **270**, 273 (1995); M. Itoh, I. Natori, S. Kubota, and K. Motoya, *J. Magn. Magn. Mater.* **140–144**, 1811 (1985); S. Yamaguchi, H. Taniguchi, H. Takagi, T. Arima, and Y. Tokura, *J. Phys. Soc. Jpn.* **64**, 1885 (1995).
- ⁷J. L. Garcia-Munoz, M. Suaaidi, M. J. Martinez-Lope, and J. Z. Alonso, *Phys. Rev. B* **52**, 13 563 (1995); P. Lacorre, J. B. Torrance, J. Pannetier, P. W. Wang, and T. C. Huang, *J. Solid State Chem.* **91**, 225 (1991); X. Bi, P. C. Eklund, and J. M. Honig, *Phys. Rev. B* **48**, 3470 (1993).
- ⁸M. Jaime, M. B. Salamon, K. L. Pettit, M. Rubinstein, R. E. Treece, J. S. Horwitz, and D. B. Chrissey, *Appl. Phys. Lett.* **68**, 1576 (1996); M. Jaime, H. Hardner, M. B. Salamon, M. Rubinstein, P. Dorsey, and D. Emin, *J. Appl. Phys.* **81**, 4958 (1997).
- ⁹H. Y. Hwang, S.-W. Cheong, P. G. Radaelli, M. Marezio, and B. Batlogg, *Phys. Rev. Lett.* **75**, 914 (1995).
- ¹⁰C. W. Searle and S. T. Wang, *Can. J. Phys.* **47**, 2703 (1969); S. T. Wang and C. W. Searle, *ibid.* **49**, 387 (1971).
- ¹¹T. Ohno, Mj. Kasai, Y. Kanke, Y. Kozono, and M. Hanazono, *Solid State Commun.* **81**, 993 (1992); S. B. Oseroff, M. Torikachvili, J. Singley, S. Ali, S. W. Cheong, and S. Schultz, *Phys. Rev. B* **53**, 6521 (1996); J. S. Ramachandran, S. M. Bhagat, J. L. Peng, and M. Rubinstein, *Solid State Commun.* **96**, 127 (1995); M. Dominguez, S. Lofland, S. M. Bhagat, A. Raychaudhuri, H. L. Ju, T. Venkatesan, and R. L. Greene, *ibid.* **97**, 193 (1996); A. K. Srivastava, C. M. Srivastava, R. Mahesh, and C. N. R. Rao, *ibid.* **99**, 161 (1996).
- ¹²P. W. Anderson and P. R. Weiss, *Rev. Mod. Phys.* **25**, 269 (1953); R. Kubo and K. Tomita, *J. Phys. Soc. Jpn.* **9**, 888 (1954).
- ¹³A. Abragam, *The Principles of Nuclear Magnetism* (Clarendon, Oxford, 1961).
- ¹⁴T. A. Kennedy, S. H. Choh, and G. Seidel, *Phys. Rev. B* **2**, 3645 (1970).
- ¹⁵S. Lofland, S. M. Bhagat, H. L. Ju, G. C. Xiong, T. Venkatesan, and R. L. Greene, *Phys. Rev. B* **52**, 15 058 (1995).
- ¹⁶J. Z. Sun, L. Krusin-Elbaum, A. Gupta, G. Xiao, and S. S. P. Parkin, *Appl. Phys. Lett.* **69**, 1002 (1996).
- ¹⁷N. F. Mott, *Conduction in Non-Crystalline Materials* (Oxford University Press, New York, 1993).
- ¹⁸M. F. Hundley and J. J. Neumeier, *Phys. Rev. B* **55**, 11 511 (1997).
- ¹⁹G. F. Dionne, *J. Appl. Phys.* **79**, 5173 (1996).
- ²⁰R. D. Shannon and C. T. Prewitt, *Acta Crystallogr. Sect. B* **25**, 925 (1969).
- ²¹S. Zhang, *J. Appl. Phys.* **79**, 4542 (1996).
- ²²G. D. Mahan, *Many-Particle Physics* (Plenum, New York, 1990); T. Holstein, *Ann. Phys. (N.Y.)* **8**, 325 (1959); **8**, 343 (1959).
- ²³A. J. Millis, P. B. Littlewood, and B. I. Shraiman, *Phys. Rev. Lett.* **74**, 5144 (1995); H. Roder, J. Zhang, and A. R. Bishop, *ibid.* **76**, 1356 (1996).
- ²⁴J. Sun, L. Krusin-Elbaum, S. Parkin, and G. Xiao, *Appl. Phys. Lett.* **67**, 2726 (1995); J. E. Nunez-Regueiro and A. M. Kadin, *ibid.* **68**, 2747 (1996).
- ²⁵S. F. Zhang (private communication).
- ²⁶N. F. Mott and H. Jones, *Theory of Properties of Metals and Alloys* (Dover, New York, 1958), Chap. VII.
- ²⁷R. Mahendhiran, S. Tiwary, and A. Raychaudhuri, *Solid State Commun.* **98**, 701 (1996).
- ²⁸A. Asamitsu, Y. Moritomo, and Y. Tokura, *Phys. Rev. B* **53**, R2952 (1996).
- ²⁹J. E. Gulley and V. Jaccarino, *Phys. Rev. B* **6**, 58 (1972).
- ³⁰H. Hasagawa, *Prog. Theor. Phys. Osaka* **21**, 483 (1959).
- ³¹S. Jin, T. H. Tiefel, M. McCormack, R. A. Fastnacht, R. Ramesh, and L. H. Chen, *Science* **264**, 413 (1994).
- ³²J. Tanaka, M. Umehara, S. Tamura, M. Tsukioka, and S. Ehara, *J. Phys. Soc. Jpn.* **51**, 1236 (1982).
- ³³K. H. Ahn, X. W. Wu, K. Liu, and C. L. Chien, *J. Appl. Phys.* **81**, 5505 (1997).